Magnetostatic response and field-controlled haloing in binary superparamagnetic mixtures

Andrey A. Kuznetsov [1,*] and Sofia S. Kantorovich [1,2]

[1]*Computational and Soft Matter Physics, Faculty of Physics, University of Vienna, Kolingasse 14-16, 1090 Vienna, Austria*
[2]*Research Platform MMM Mathematics-Magnetism-Material, University of Vienna, Oskar-Morgenstern-Platz 1, 1090 Vienna, Austria*

Nowadays, magnetoresponsive soft materials, based not simply on magnetic nanoparticles but rather on multiple components with distinct sizes and magnetic properties in both liquid and polymeric carriers, are becoming more and more widespread due to their unique and versatile macroscopic response to an applied magnetic field. The variability of the latter is related to a complex interplay of the magnetic interactions in a highly nonuniform internal field caused by spatial inhomogeneity in multicomponent systems. In this work, we present a combined analytical and simulation study of binary superparamagnetic systems containing nanoclusters and dispersed single-domain nanoparticles in both liquid and solid carrier matrices. We investigate the equilibrium magnetic response of these systems for wide ranges of concentrations and interaction energies. It turns out that, while the magnetization of a binary solid can be both above and below that of an ideal superparamagnetic gas, depending on the concentration of the dispersed phase and the interparticle interactions, the system in a liquid carrier is highly magnetically responsive. In liquid, a spatial redistribution of the initially homogeneously dispersed phase in the vicinity of the nanocluster is observed, an effect that is reminiscent of the so-called haloing effect previously observed experimentally on micro- and milliscales.

I. INTRODUCTION

Magnetic soft matter is a family of artificially synthesized materials based on a distributed system of magnetic particles embedded in a nonmagnetic carrier matrix. Notable members of this family are ferrofluids [1], magnetorheological fluids [2], ferrogels [3], and magnetoactive elasomers [4]. The behavior and properties of these systems can be controlled using applied magnetic fields, which makes them highly attractive in various branches of nanotechnology and nanomedicine. Examples of applications include soft crawling robots [5], tissue engineering scaffolds [6], adaptive dampers and seals [7], ferrofluid cooling systems [8], magnetic lubricants [9], targeted drug delivery systems [10], magnetic hyperthermia of cancer [11], and magnetic particle imaging [12].

Modern methods of magnetic soft matter synthesis have achieved tremendous success. In particular, particles can vary greatly in size and can have very different internal magnetic structures. The common types of particles are single-domain ferro- and ferrimagnetic nanoparticles with linear sizes ~ 10 nm [13], dense clusters of single-domain nanocrystals (magnetic "nanoflowers" [14] and "multicore nanoparticles" [15,16] with a size of the order of $\sim 10^2$ nm), and multidomain microparticles with low or high coercivity [17]. Recently, multicomponent systems, which simultaneously employ several types of magnetic particles, attracted a lot of scientific attention. For instance, these are hybrid elastomers containing both magnetically soft and hard microparticles [18]. Reportedly, they allow for a much larger degree of magnetomechanical fine tuning than analogous one-component systems [19]. In Ref. [20], an elastic sphere filled with magnetically saturated colloidal particles of two different sizes was considered; it was shown that for certain spatial arrangements of particles, variation in the quantitative ratio between small and large particles can lead to qualitative changes in the system's overall deformation response. Another example is bimodal magnetorheological fluids, which consist of magnetic microparticles submerged in a nanodispersed ferrofluid [21]. They are considered to be an improved substitution for conventional magnetorheological fluids due to their superior colloidal stability and sedimentation behavior [22,23]. Recently, a novel type of binary ferrofluid containing a mixture of magnetically hard and magnetically soft nanoclusters was experimentally investigated in Ref. [24]. Even some samples of traditional ferrofluids are known to contain a fraction of large nanoclusters, which results in a substantial alteration of their magnetic, mass-transport, and rheological properties [25–28].

The more magnetic soft matter systems that contain two types of magnetic components are developed, the clearer the demand to understand the fundamental interplay between interactions of those components and their impact on the system's overall magnetic response becomes. The latter is of particular importance because it forms the basis for efficient usage of these materials.

Here, we will focus mainly on composite materials that are based on single-domain fine particles. It is known that if the internal anisotropy energy of such particles is comparable to or smaller than the energy of thermal fluctuations (which is common for iron oxide nanoparticles [13]), then the average ensemble magnetization in zero field is zero. As the field increases, the magnetization will nonlinearly and reversibly grow towards the saturation value. Such behavior is known

*andrey.kuznetsov@univie.ac.at

as "*superparamagnetism*," and corresponding materials can be referred to as "*superparamagnetic*" [29]. While interactions in one-component superparamagnetic systems are very important, in both liquid [30,31] and solid [32,33] carriers, the situation becomes even more complex if the material is multicomponent. Clear evidence of this is the direct and inverse ferrofluid emulsions that are binary systems with only one magnetic component [34–37]. Here, the nonuniformity of the internal magnetic field inside the sample leads to a very sophisticated magnetic response. It is, however, clear that the internal field gradients will become even stronger and more important if a true binary magnetic material is addressed. So far, a detailed description, as well as a fundamental understanding of the magnetization processes in such materials, is not available in the scientific literature. This work aims at filling this gap and puts forward a combined analytical-computational study of a system containing both large superparamagnetic nanoclusters (the sources of strong internal field and spatial inhomogeneity) and a dispersed phase of single-domain superparamagnetic particles that are forced to react to the perturbations created by the cluster. As long as we expect a drastic change depending on the carrier, we investigate two extreme cases: the disperse phase is either frozen in space, maintaining only the rotational degrees of freedom, mimicking a material based on a rubber-like rigid matrix, or the whole system is immersed in a liquid where the disperse phase can freely diffuse. It turns out that in the latter, a pronounced gathering of the dispersed phase in the vicinity of the nanocluster is observed, causing qualitative changes in the magnetization behavior.

This paper is organized as follows. First, we describe the model in detail in Sec. II. In Sec. III, we adapt the analytical approach developed by Subbotin [35,36] and calculate the magnetization of our binary system. The results and discussion in Sec. IV are split according to the carrier: we discuss a solid matrix in Sec. IV A; a liquid carrier is studied in Secs. IV B and IV C. In particular, spatial redistribution of the dispersed phase is investigated in Sec. IV C. The summary and a short outlook are provided in Sec. V.

II. MODEL OF A BINARY SUPERPARAMAGNETIC MIXTURE

The system under consideration is an isolated magnetic nanocluster embedded in a superparamagnetic medium (see Fig. 1). The system is subjected to an external uniform magnetic field $\vec{H}_0$ and thermostated at a constant temperature T. The nanocluster is modeled as a sphere of diameter D_{cl} filled with N_{in} spherical magnetic particles of diameter d. Particles are distributed within the cluster randomly and uniformly, without overlapping; their volume fraction is

$$\varphi_{\mathrm{in}} = N_{\mathrm{in}} \frac{v}{V_{\mathrm{cl}}} = N_{\mathrm{in}} \left(\frac{d}{D_{\mathrm{cl}}} \right)^3, \quad (1)$$

where $v = (\pi/6)d^3$ and $V_{\mathrm{cl}} = (\pi/6)D_{\mathrm{cl}}^3$ are volumes of the particle and the nanocluster, respectively. Positions of particles within the nanocluster are rigidly fixed. Particles are assumed to be single domain and magnetically isotropic (the validity of this approximation is commented on in
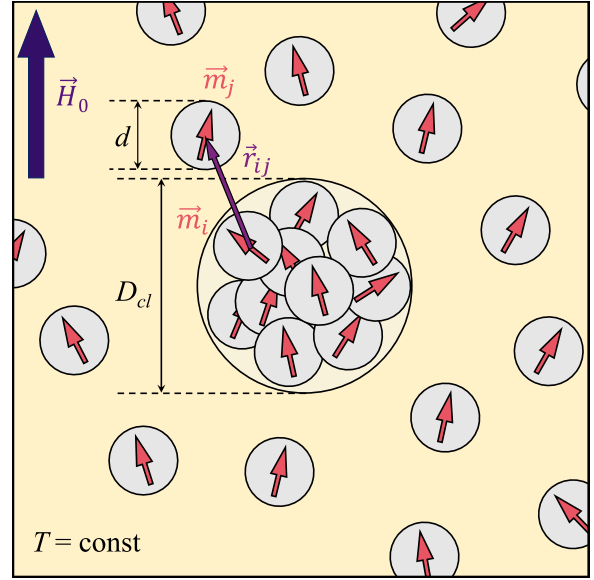

FIG. 1. Schematic representation of the investigated system.

Appendix A). Each particle has a magnetic moment $\vec{m}$ whose magnitude is fixed, but its orientation can change under the influence of an applied magnetic field, dipolar magnetic fields created by other magnetic moments in the system, and thermal fluctuations. As a result, the nanocluster as a whole will exhibit superparamagnetic behavior according to the definition introduced in the previous section. It does not have a net magnetic moment in the absence of an applied field but will be nonlinearly magnetized if the field is turned on [38]. The superparamagnetic medium surrounding the nanocluster is modeled in a similar fashion. It consists of N_{ex} magnetically isotropic spherical single-domain particles, which are exactly the same as particles that constitute the cluster; that is, they also have diameter d and rotatable magnetic moment $\vec{m}$. The particle volume fraction in the medium is

$$\varphi_{\mathrm{ex}} = N_{\mathrm{ex}} \frac{v}{V_{\mathrm{tot}} - V_{\mathrm{cl}}}, \quad (2)$$

where V_{tot} is the total system volume. Magnetic nanoparticles in the medium always retain their rotational degrees of freedom.

The interaction of magnetic moments with the external field is governed by the Zeeman potential

$$U_Z = -\mu_0 (\vec{m} \cdot \vec{H}_0), \quad (3)$$

where μ_0 is the magnetic permeability of the vacuum. Additionally, each pair of particles interacts via the magnetic dipole-dipole potential

$$U_{dd}(i, j) = \frac{\mu_0}{4\pi} \left[\frac{(\vec{m}_i \cdot \vec{m}_j)}{r_{ij}^3} - \frac{3(\vec{m}_i \cdot \vec{r}_{ij})(\vec{m}_j \cdot \vec{r}_{ij})}{r_{ij}^5} \right], \quad (4)$$

where $\vec{m}_i$ and $\vec{m}_j$ are magnetic moments of two particles and $\vec{r}_{ij}$ is the vector connecting their centers. We use two dimensionless energy parameters to characterize these magnetic interactions. The first one is the Langevin parameter

$$\xi_0 = \frac{\mu_0 m H_0}{k_B T}, \quad (5)$$

which is the ratio of the Zeeman energy to the thermal energy $k_B T$, where k_B is the Boltzmann constant and $m = |\vec{m}_i|$. For a 10 nm magnetite grain (with saturation magnetization $M_s = 450$ kA/m), $\xi_0 = 1$ corresponds to $H \simeq 14$ kA/m at room temperature. The second parameter is the so-called dipolar coupling constant

$$\lambda = \frac{\mu_0}{4\pi} \frac{m^2}{d^3 k_B T}, \tag{6}$$

which is the characteristic energy scale of two adjacent particles whose dipoles are aligned head to tail divided by $k_B T$ and calculated per particle. At $T = 300$ K, this parameter for a pair of magnetite grains will roughly go from $\lambda \sim 1$ to $\lambda \sim 10$ as their diameter increases from 10 to 20 nm.

Modeling of different carriers will be done by changing the way we treat the translational degrees of freedom of our particles. In a solid carrier matrix (SCM), single-domain particles surrounding the cluster will be randomly distributed in the medium and would not be able to move (just like the particles that constitute the nanocluster itself). In a liquid carrier matrix (LCM), particles will be subjected to a translational Brownian motion and could change their position relative to the nanocluster. They are assumed to be sterically stabilized and are not allowed to overlap. Of course, in a liquid the nanocluster should undergo the Brownian motion as well. However, we can make use of the fact that the characteristic timescales for three-dimensional (3D) Brownian motion of a cluster and a particle, $\tau_{cl} = 3\eta V_{cl}/k_B T$ and $\tau_p = 3\eta v/k_B T$, respectively (η is the carrier viscosity), are very different. Indeed, if $D_{cl}/d \sim 10$, the cluster motion is three orders of magnitude slower than that of surrounding particles. Thus, in LCM simulations the cluster will be treated as if its position is fixed.

Our main quantities of interest in this work are the normalized equilibrium magnetic moment of the nanocluster

$$\vec{\mathcal{M}}_{cl} = \left\langle \sum_{i=1}^{N_{in}} \vec{m}_i \right\rangle \frac{1}{m N_{in}} \tag{7}$$

and the total normalized magnetic moment of the whole system

$$\vec{\mathcal{M}}_{tot} = \left\langle \sum_{i=1}^{N_{tot}} \vec{m}_i \right\rangle \frac{1}{m N_{tot}}, \tag{8}$$

where $N_{tot} = N_{in} + N_{ex}$ is the total number of particles in the system and $\langle \cdots \rangle$ denotes an ensemble average.

In this work, we use both analytical theory (Sec. III) and Langevin dynamics simulations (for details, see Appendix B). However, already at this point, it is important to specify that the system in simulations is subjected to 3D periodic boundary conditions. It approximately corresponds to a suspension of nanoclusters with a nanocluster volume fraction

$$\Phi_{cl} = \frac{V_{cl}}{V_{tot}} = \left(1 + \frac{\varphi_{in}}{\varphi_{ex}} \frac{N_{ex}}{N_{in}} \right)^{-1}. \tag{9}$$

We will consider systems with $N_{in} = 500$ and $N_{ex} = 2500$. Particle concentration in the cluster is always $\varphi_{in} = 0.3$ (correspondingly, $D_{cl} \simeq 12d$), while the concentration of the surrounding medium will be changed from a small value

of $\varphi_{ex} = 0.002$ to $\varphi_{ex} = 0.15$. Correspondingly, the cluster concentration will change from $\Phi_{cl} \simeq 0.0013$ to $\Phi_{cl} \simeq 0.09$. Magnetic interaction parameters will also vary over wide ranges: $1 \leqslant \lambda \leqslant 5$ and $0 \leqslant \xi_0 \leqslant 5$.

III. MAGNETIC RESPONSE THEORY

In this section, we will summarize the works of Subbotin on inverse ferroemulsions [35,36] and adapt them to binary superparamagnetic mixtures. Let us consider a suspension of spherical magnetizable bodies (clusters) in a magnetizable medium with a relative magnetic permeability μ_{ex}. Assume that the volume fraction of clusters is Φ_{cl} and they are made of some material with relative magnetic permeability μ_{in}. According to Refs. [35,36], the field inside clusters is homogeneous and parallel to the external field; its magnitude is given by

$$H_{in} = H_0 \frac{1}{1 + (1 - \Phi_{cl})\kappa \left(\frac{\mu_{in}}{\mu_{ex}} - 1 \right)}, \tag{10}$$

where κ is the cluster demagnetization factor. For a sphere, $\kappa = 1/3$. The field in the surrounding medium is

$$H_{ex} = H_0 \left[1 + \frac{\Phi_{cl} \kappa \left(\frac{\mu_{in}}{\mu_{ex}} - 1 \right)}{1 + (1 - \Phi_{cl})\kappa \left(\frac{\mu_{in}}{\mu_{ex}} - 1 \right)} \right]. \tag{11}$$

Permeabilities, in general, can be considered nonlinear functions of the field:

$$\mu_{in} = 1 + \frac{M_{in}(H_{in})}{H_{in}}, \tag{12}$$

$$\mu_{ex} = 1 + \frac{M_{ex}(H_{ex})}{H_{ex}}, \tag{13}$$

where M_{in} and M_{ex} are magnetizations of the cluster material and of the medium, respectively. The total magnetization of the system is

$$M_{tot} = \Phi_{cl} M_{in}(H_{in}) + (1 - \Phi_{cl}) M_{ex}(H_{ex}). \tag{14}$$

Normalized magnetic moments then can be found as

$$\mathcal{M}_{cl} = \frac{M_{in} V_{cl}}{m N_{in}}, \quad 0 \leqslant \mathcal{M}_{cl} \leqslant 1, \tag{15}$$

$$\mathcal{M}_{tot} = \frac{M_{tot} V_{tot}}{m N_{tot}}, \quad 0 \leqslant \mathcal{M}_{tot} \leqslant 1. \tag{16}$$

Later on, the set of equations (10)–(16) will be referred to as the binary mixture magnetization (BMM) model.

The key assumption of the BMM is that magnetic field in the medium H_{ex} is a sum of the external field H_0 and some average field that is created by all magnetized clusters, distributed in the system. This latter field is assumed to be uniform, and so is H_{ex} itself. However, it is known that the local magnetic field (and subsequently μ_{ex}) in the vicinity of a magnetized spherical body is nonuniform [13]. Thus, Eqs. (10) and (11) are only an approximation. The BMM, however, converges to a well-known Maxwell-Wagner formula for the initial permeability of a binary dielectric mixture [39]. In the weak-field limit, it also shows good agreement with experimental data on the effective permeability of
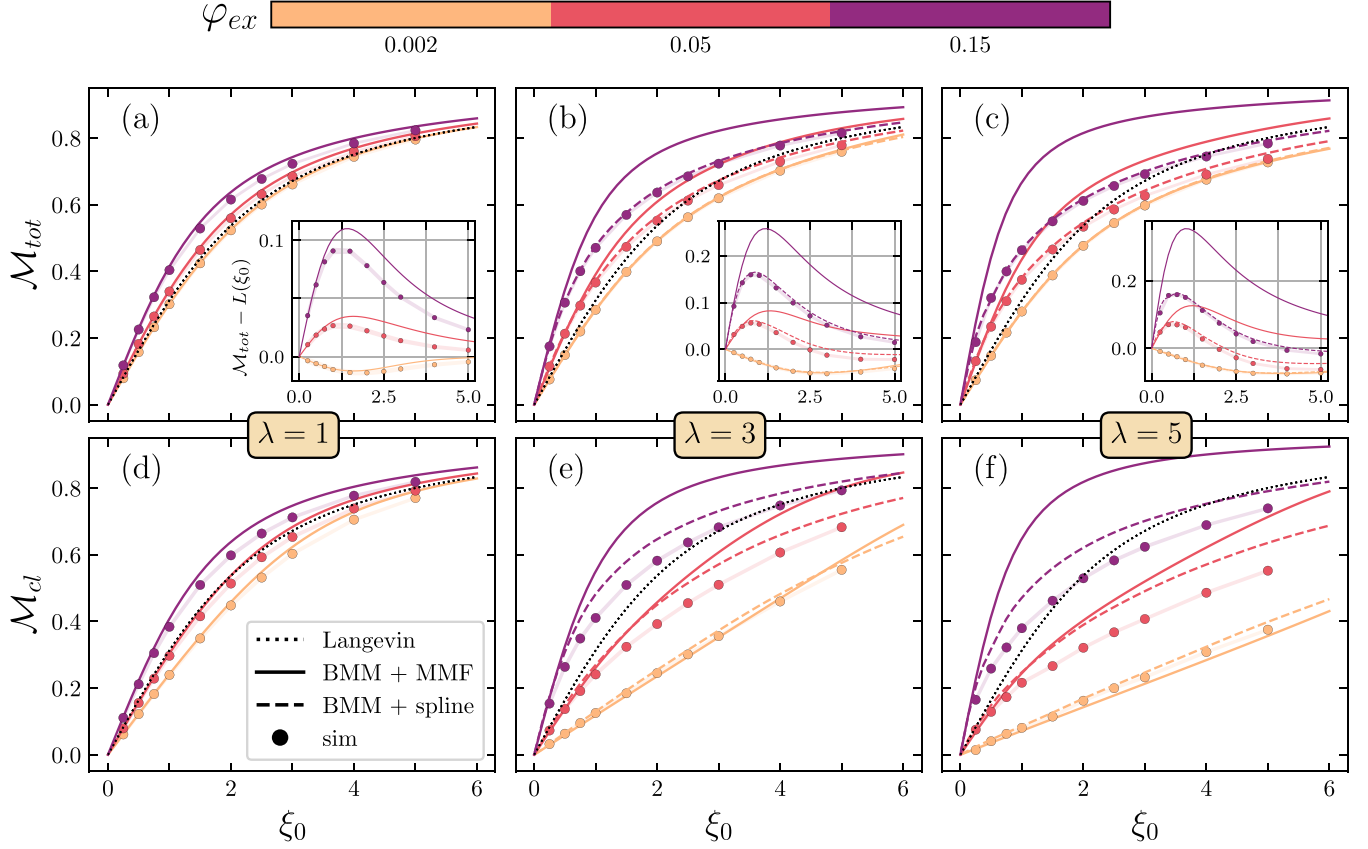
FIG. 2. Equilibrium magnetization curves of a superparamagnetic mixture in a solid carrier. The top row demonstrates dependences of a normalized magnetization (or, identically, of a normalized magnetic moment) of the whole system $\mathcal{M}_{\text{tot}}$ on the Langevin parameter ξ_0. Insets in [(a)–(c)] show the difference between $\mathcal{M}_{\text{tot}}$ values from the corresponding panels and the Langevin function $L(\xi_0)$. The latter is indicated in the main panels with dotted lines. The bottom row shows corresponding values of the cluster normalized magnetic moment $\mathcal{M}_{\text{cl}}$. Different columns correspond to different dipolar coupling parameters: (a) and (d) $\lambda = 1$, (b) and (e) $\lambda = 3$, and (c) and (f) $\lambda = 5$. The particle volume fraction in the surrounding medium φ_{ex} is indicated by color (see the color bar). Simulation results are shown by circles (transparent lines connecting them are guides for the eye), and solid lines are predictions from the BMM model [Eqs. (10)–(16)] combined with MMF expressions for magnetic permeabilities [Eqs. (20) and (21)]. Dashed lines are "corrected" BMM predictions with permeability values directly extracted from auxiliary simulations of one-component superparamagnetic systems rather than from MMF.

inverse ferroemulsions. This model, however, overestimates experimental results slightly as the applied field increases. The applicability of the BMM to our system is to be determined.

In order to close the set of BMM equations, some explicit expressions for magnetization curves $M_{\text{in}} = M_{\text{in}}(H_{\text{in}})$ and $M_{\text{ex}} = M_{\text{ex}}(H_{\text{ex}})$ are required. For this purpose, the so-called modified mean-field (MMF) theory can be used. It was initially developed to describe static magnetic properties of concentrated ferrofluids [40,41]. Subsequently, the approach was extended for the description of the ferrofluid dynamic response [31] as well as magnetic properties of single-domain nanoparticle ensembles immobilized in a solid nonmagnetic matrix [32]. Reference [36] also used the first-order MMF to describe the magnetic component of an inverse ferroemulsion. Within a more accurate second-order MMF approach [42], magnetization of a one-component superparamagnetic material can be written as

$$M(H) = M_s L\left[\xi_{\text{eff}}\left(\frac{\mu_0 m H}{k_B T}, \chi_L\right)\right], \qquad (17)$$

$$\xi_{\text{eff}}(\xi, \chi_L) = \xi + \chi_L[1 + \chi_L L'(\xi)/16]L(\xi), \qquad (18)$$

$$L(\xi) = \coth \xi - 1/\xi, \qquad (19)$$

where $M_s = (6/\pi d^3)m\varphi$ is the material saturation magnetization, φ is the particle volume fraction, $\chi_L = 8\lambda\varphi$ is the so-called Langevin susceptibility, $L(\xi)$ is the Langevin function that describes the magnetic response of an ensemble of noninteracting dipoles (i.e., at $\chi_L \ll 1$), $L'(\xi) = dL(\xi)/d\xi$, ξ_{eff} is the effective dimensionless field that acts locally on an arbitrary chosen particle in an ensemble with dipole-dipole interactions. If we assume that both components of our binary mixture can be described by the MMF, permeabilities can be written down as

$$\mu_{\text{in}} = 1 + 3\chi_L^{\text{in}} \frac{L\big(\xi_{\text{eff}}(\xi_{\text{in}}, \chi_L^{\text{in}})\big)}{\xi_{\text{in}}}, \qquad (20)$$

$$\mu_{\text{ex}} = 1 + 3\chi_L^{\text{ex}} \frac{L\big(\xi_{\text{eff}}(\xi_{\text{ex}}, \chi_L^{\text{ex}})\big)}{\xi_{\text{ex}}}, \qquad (21)$$

where $\chi_L^{\text{in}} = 8\lambda\varphi_{\text{in}}$, $\chi_L^{\text{ex}} = 8\lambda\varphi_{\text{ex}}$, $\xi_{\text{in}} = \mu_0 m H_{\text{in}}/k_B T$, and $\xi_{\text{ex}} = \mu_0 m H_{\text{ex}}/k_B T$.

IV. RESULTS AND DISCUSSION

A. Equilibrium magnetization of a mixture in a solid carrier

Magnetization curves for a superparamagnetic cluster embedded in a solid matrix with immobilized nanoparticles are shown in Fig. 2 for different values of λ and φ_{ex}. The first noticeable feature of magnetization curves is that at any given λ an increase in φ_{ex} leads to a qualitative change in how the system magnetization relates to the Langevin function. Langevin magnetization corresponds to a system of non-interacting dipoles. So if the normalized magnetization is lower than corresponding Langevin value, dipole-dipole interactions hinder the overall magnetic response. Conversely, magnetization higher than the Langevin value indicates that dipole-dipole interactions play a reinforcing role. It is known that the equilibrium magnetostatic response of superparamagnetic clusters in an empty space always lies below the Langevin curve [38]; this is the result of the demagnetization effect. Similar behavior is observed in our system for a cluster in a diluted medium with $\varphi_{\mathrm{ex}} = 0.002$. However, as the concentration of particles in the surrounding medium increases (and as the magnetic permeability of the medium μ_{ex} becomes closer to the permeability of the cluster μ_{in}), demagnetization effects slowly disappear—magnetization of both the cluster and the mixture eventually becomes larger than the Langevin value. Interestingly enough, at $\varphi_{\mathrm{ex}} \geqslant 0.05$ and $\lambda \geqslant 3$ the impact of dipole-dipole interactions on the mixture magnetization depends nonmonotonically on the field; while the initial section of the magnetization curve is larger than that of the Langevin function, simulation points eventually fall below $L(\xi)$ in the saturation regime.

As for the theoretical predictions, it is seen that the combination of the BMM and MMF gives very accurate predictions for the initial slope of magnetization curves in the whole investigated parameter range. However, as the field increases, theory and simulation data start to diverge rapidly. The larger φ_{ex} and/or λ reinforce the discrepancy. Theoretical (solid) curves in Fig. 2 are always above simulation points at $\xi_0 > 1$. At $\varphi_{\mathrm{ex}} = 0.15$ and $\lambda = 5$, the error between numerical and theoretical values of the mixture magnetization reaches almost 20% of the corresponding saturation value.

To understand the reason for the discrepancy between theory and simulations, a set of auxiliary simulations was performed. We simulated a one-component ensemble of immobilized nanoparticles randomly and uniformly distributed in a standard cubic box with 3D periodic boundary conditions. An ensemble of $N = 2000$ particles was considered. Using simulation data, the nonlinear magnetic permeability of the ensemble was calculated as a function of the field ξ at different λ and particle volume fractions φ. The results are demonstrated in Fig. 3 in comparison with MMF predictions. It can be seen that while MMF mostly predicts correct zero-field permeability values, at large fields it overestimates μ. In more detail this feature of immobilized superparamagnetic ensembles was discussed in Ref. [38]. To take it into account, the following procedure was performed. The calculated permeability of a one-component system was interpolated (with cubic splines) and then put in BMM instead of MMF predictions [Eqs. (20) and (21)]. The results of this procedure are shown in Fig. 2 with dashed lines. We can see
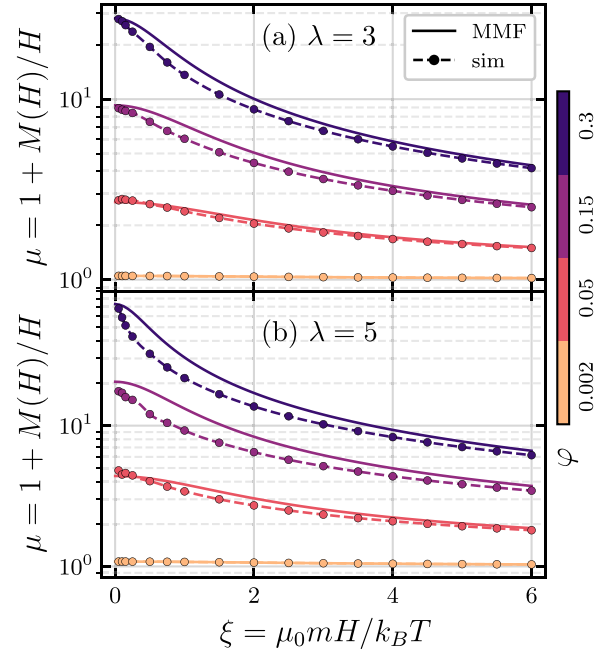

FIG. 3. Field dependences of the magnetic permeability for a one-component ensemble of randomly distributed immobilized magnetic nanoparticles. Solid lines are MMF theory predictions [Eqs. (17) and (18)], and circles are simulation results. Different panels correspond to different dipolar coupling constants: (a) $\lambda = 3$ and (b) 5. Particle volume fractions are indicated by color.

that the accuracy of BMM with "corrected" permeabilities improves drastically. New theoretical curves closely follow $\mathcal{M}_{\mathrm{tot}}$ dependences. The magnetization curves for the cluster still overestimate numerical results, but they are much better than the MMF for $\lambda \geqslant 3$ and $\varphi_{\mathrm{ex}} \geqslant 0.05$. The probable reason for the remaining discrepancy is the inherent BMM assumption that the magnetic field H_{ex} and permeability of the surrounding medium μ_{ex} are constant and uniform in the cluster's vicinity, which is not correct at large enough applied fields [13]. Thus, the agreement with simulation potentially can be improved only by directly solving a nonlinear magnetostatic boundary-value problem and correctly determining the magnetic field distribution in the system. However, this task is beyond the scope of the present paper.

B. Equilibrium magnetization of a mixture in a liquid carrier

Now let us consider a different type of a binary mixture—a superparamagnetic nanocluster submerged in a suspension of magnetic nanoparticles in a nonmagnetic liquid matrix. Essentially, a nanocluster in a ferrofluid or in a very loose gel in which the cluster is too large to diffuse but the dispersed phase is not constrained [43]. The magnetization curves for this case are shown in Fig. 4. The first thing that is seen here is that the magnetization of the mixture and the cluster are larger than corresponding SCM values for every set of investigated parameters. A noticeable feature of the previously considered SCM is that $\mathcal{M}_{\mathrm{tot}}$ at large φ_{ex} can be higher than the corresponding Langevin value in weak fields but smaller than the Langevin value in strong fields. The role of dipole-dipole interactions changes as the field increases. For LCM,
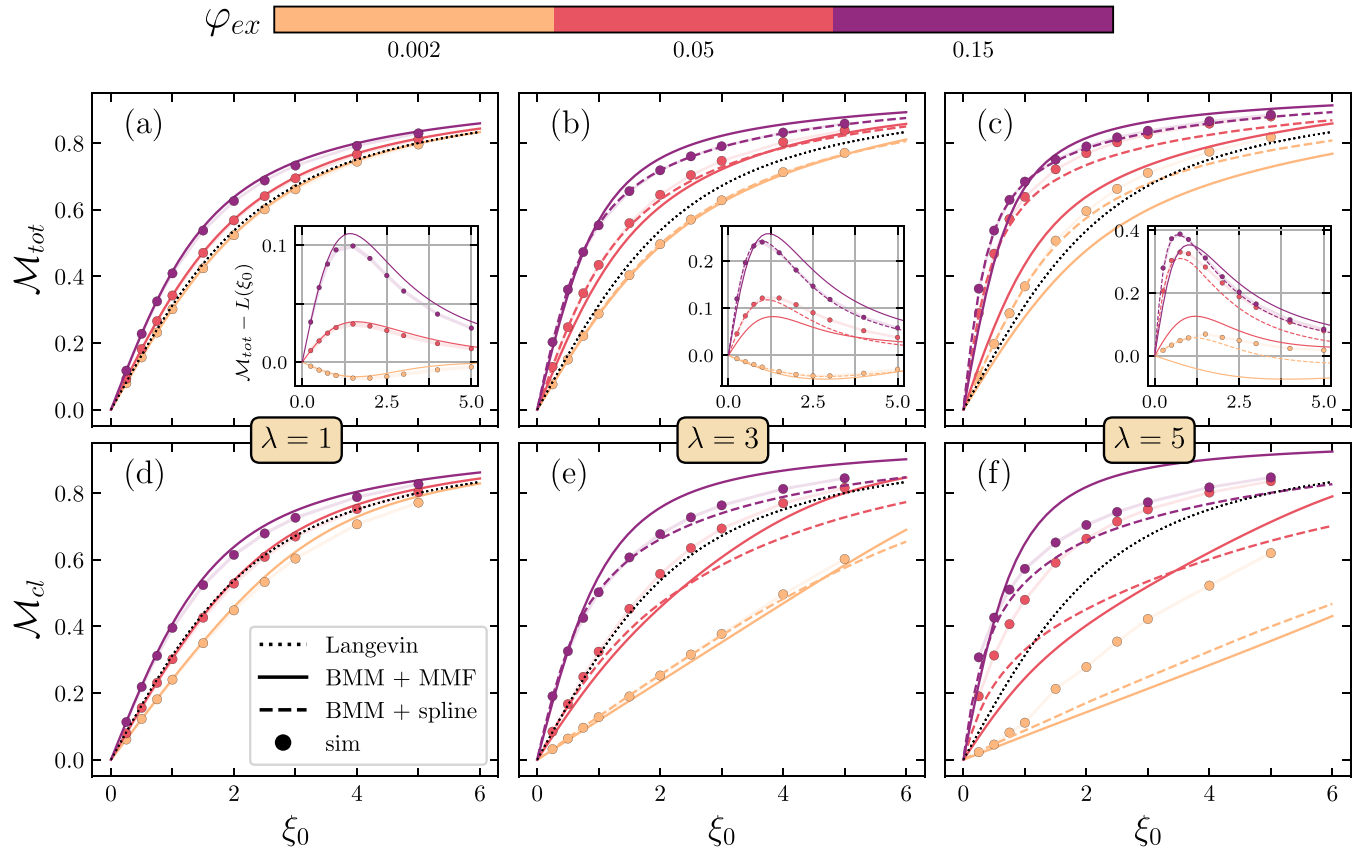
FIG. 4. Equilibrium magnetization curves for a superparamagnetic mixture in a liquid carrier. The notation is identical to that in Fig. 2. Note that colored solid curves corresponding to MMF predictions are also exactly the same as in Fig. 2.

this feature is no longer present—there is no crossing of the Langevin curve, at least not at $\xi_0 \leqslant 5$.

MMF does not make any distinctions between liquid and solid superparamagnetic ensembles; thus, theoretical curves in Fig. 4 are exactly the same as in Fig. 2. At $\lambda = 1$, these curves actually describe simulation data for LCM quite well, better than the data for SCM [compare insets in Figs. 2(a) and 4(a)]. But already at $\lambda = 3$ the agreement breaks down. Surprisingly, the error does not increase with φ_{ex} as in SCM case—the strongest disagreement between theory and simulations takes place at intermediate and low concentrations. For $\lambda = 3$ and $\varphi_{ex} = 0.05$, theoretical predictions are incorrect for both the initial and saturation portions of the LCM magnetization curve [Figs. 4(b) and 4(e)]. At $\lambda = 5$, the strongest disagreement takes place at even smaller concentrations, $\varphi_{ex} = 0.002$ [Figs. 4(c) and 4(f)].

In order to improve the agreement, the same procedure was employed as for SCM. Namely, an auxiliary set of simulations of a one-component superparamagnetic system was performed. This time, the one-component system was a liquid suspension of single-domain particles. The results for a nonlinear magnetic permeability of this system at different particle concentrations and dipolar coupling constants are given in Fig. 5. Comparing Fig. 5 to Fig. 3, we can see that the relations between actual permeability and MMF predictions for liquid and solid one-component superparamagnets are completely opposite. For solid systems, zero-field permeabilities are correctly described by MMF, but

the theory overestimates the magnetic response as the field increases. These features of solid superparamagnets are well documented in the literature [38,44]. For a liquid, zero-field permeabilities are larger than MMF predictions, but in strong fields the agreement significantly improves. This behavior can be attributed to the particle self-assembly, which is not taken into account within the MMF framework. It is known that magnetic particles with sufficiently strong dipole-dipole interactions tend to form chain-like aggregates in viscous [45] and even soft elastic environments [46]. In monodisperse ferrofluids, the chain formation increases the initial magnetic response [47], but under the saturation condition the influence of chains on the magnetization reduces [48].

Once again, numerically obtained permeability curves were interpolated with cubic splines and then used within the BMM approach instead of MMF predictions [Eqs. (20) and (21)]. The results of this correction are shown in Fig. 4 with dashed lines. Unfortunately, the correction no longer gives the same accuracy boost as for SCM. In fact, it improves only the initial slope of the magnetization curves. But at large fields, simulation results persistently lie above the predictions of the corrected BMM. This is most clearly demonstrated by $\mathcal{M}_{tot}$ and $\mathcal{M}_{cl}$ dependences for $\lambda = 5$ and $\varphi_{ex} = 0.002$ [Figs. 4(c) and 4(f)].

So it can be deduced that some qualitative change is happening in LCM system as the field increases:

(i) This change leads to a significant increase of normalized magnetic moments $\mathcal{M}_{tot}$ and $\mathcal{M}_{cl}$.
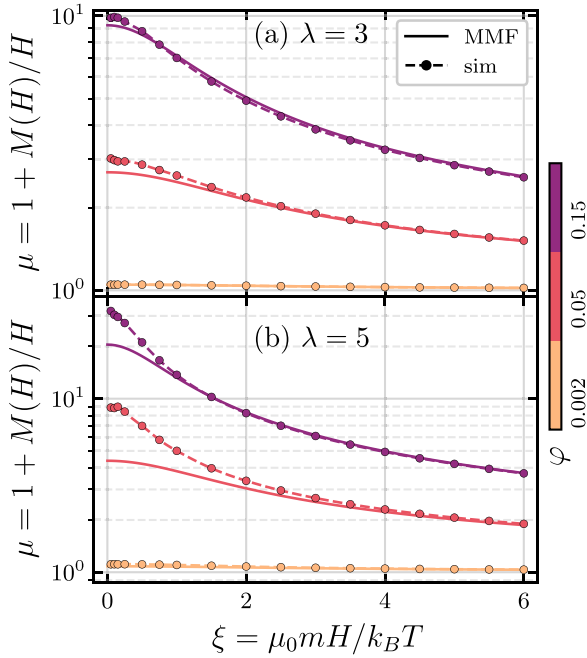
FIG. 5. Field dependences of the magnetic permeability for a one-component ensemble of magnetic nanoparticles suspended in a liquid matrix (i.e., particles are subjected to a translational Brownian motion). The notation is identical to that in Fig. 3.

(ii) It cannot be explained within the BMM approach.

(iii) It is more pronounced at larger λ and smaller φ_{ex}.

(iv) It does not take place in the SCM.

To get a better understanding of what is happening here, a deeper analysis of the system microstructure is presented below.

C. Field-controlled haloing in a liquid carrier

Let us look closely at the behavior of the simulated LCM system at $\lambda = 5$ and $\varphi_{\text{ex}} = 0.002$, i.e., in the parameter ranges where the deviations from theoretical magnetization curves are most pronounced. Corresponding simulation snapshots are collected in Fig. 6 for different values of the applied field strength. At a relatively small field, $\xi_0 = 1$, free nanoparticles form chain-like structures, as expected at $\lambda = 5$ [47]. The presence of a cluster does not produce any clearly visible effects on the system microstructure. However, already at

$\xi_0 = 2$ and, especially, at $\xi_0 = 4$, a significant change takes place: particles (or, rather, particle chains) start to concentrate near the nanocluster poles, forming clouds stretched along the field direction.

The described phenomenon is qualitatively reminiscent of the so-called *haloing* effect, experimentally observed in bimodal magnetorheological fluids [21,49]. The only difference is that in the latter systems superparamagnetic nanoclusters form thick clouds (or *halos*) around a magnetizable microsphere. On an even larger scale the phenomenon was reproduced in Ref. [50]: the authors observed the condensation of drop-like aggregates of a phase-separated ferrofluid on the surface of a millimeter-sized iron sphere. The physical reason behind this halo formation in both cases is the phenomenon of magnetophoresis, i.e., the motion of magnetic nanoparticles in a gradient magnetic field [27,51]. The source of the inhomogeneous field in our problem is the magnetized nanocluster [13]. The stronger the applied field is, the stronger the cluster's own field gradient is. This gradient is directed towards poles of the cluster, where free nanoparticles and nanoparticle chains tend to accumulate.

It is known that the transport of magnetic nanoparticles in a viscous medium is affected strongly by interparticle interactions [52,53]. Namely, dipole-dipole interactions, controlled by λ, act as effective attraction between particles. They decrease the gradient diffusion coefficient of the system and make it much easier to create a highly inhomogeneous particle distribution with a given applied field. The effect of dipole-dipole interactions on particle transport is typically most pronounced at intermediate average concentrations $\varphi \leqslant 0.1$. In denser systems, the steric repulsion (i.e., the excluded volume effect) starts to dominate and substantially increases the gradient diffusion coefficient. To put it simply, it is hard to create a noticeable concentration gradient in a highly concentrated system. All these theoretical considerations are well illustrated and validated by the LCM concentration maps shown in Fig. 7. First, halo concentration increases with λ. At $\varphi_{\text{ex}} = 0.002$ and $\lambda = 5$, the *local* concentration of particles near cluster poles is actually comparable to the cluster concentration itself ($\varphi_{\text{in}} = 0.3$) and two orders of magnitude higher than near the cluster "flanks." Thus, the situation can be interpreted as follows: the cluster, which is spherical in small fields, starts to absorb free particles with increasing ξ_0 and turns into an elongated aggregate aligned with the field. As the aggregate shape changes, its demagnetization factor
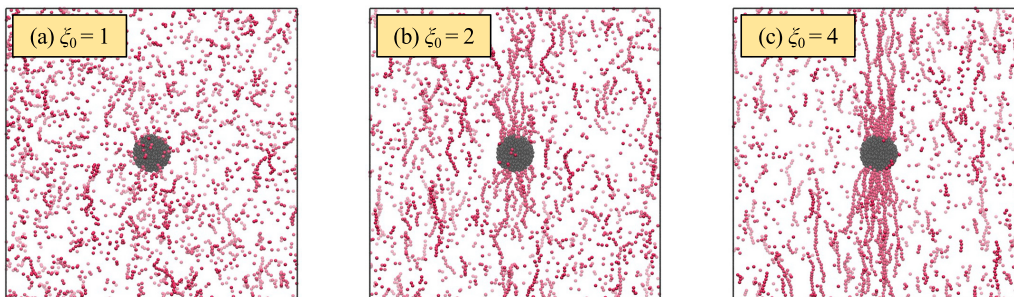

FIG. 6. Simulation snapshots of the system in a liquid carrier at $\varphi_{\text{ex}} = 0.002$ and $\lambda = 5$. Different panels correspond to different Langevin parameters: (a) $\xi_0 = 1$, (b) 2, and (c) 4. Applied field is oriented vertically.
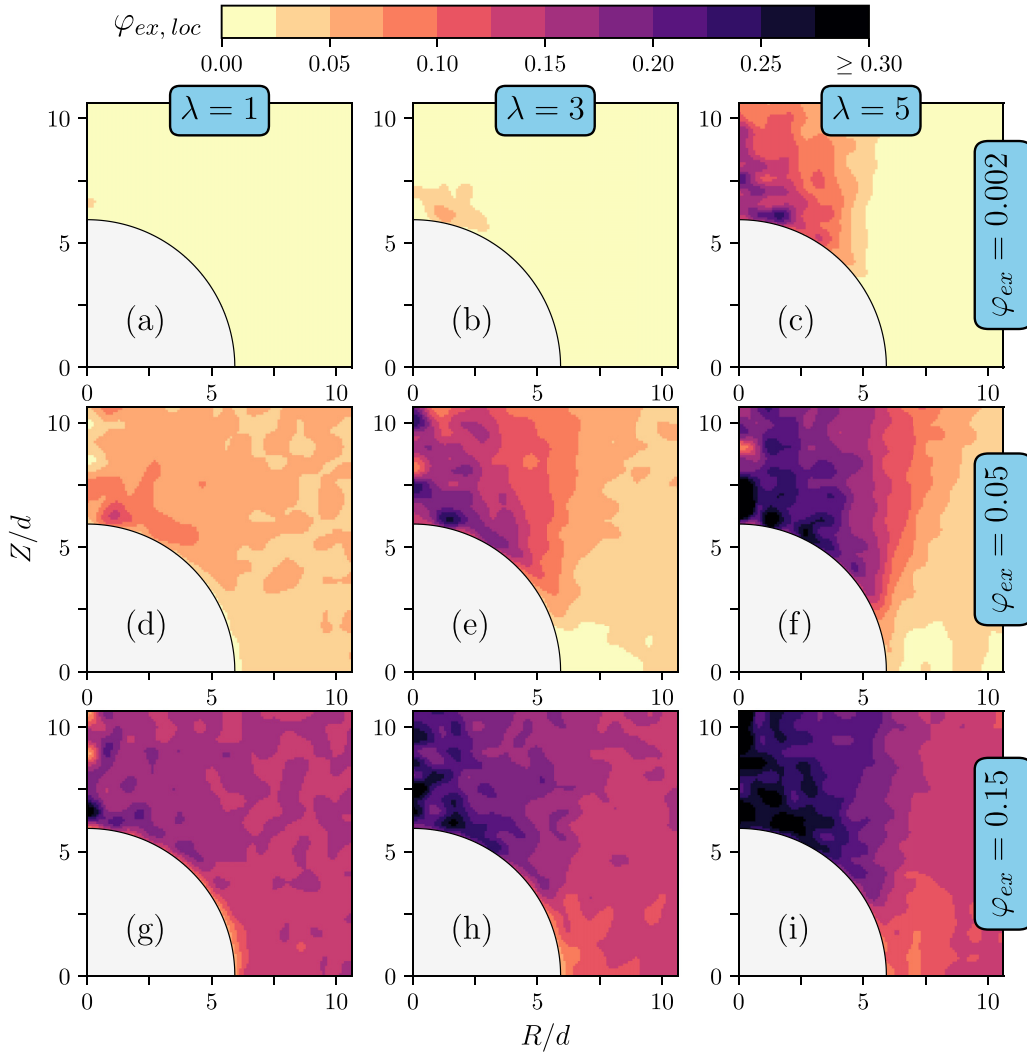
FIG. 7. Local particle volume fraction $\varphi_{ex,\,loc}$ in the vicinity of the cluster at $\xi_0 = 3$. Numerical values of $\varphi_{ex,\,loc}$ are indicated by the color (see color bar); the cluster itself is colored gray. Maps are constructed using space- and time-averaged data from 3D Langevin dynamics simulations. They are plotted in cylindrical coordinates (R, Z) with the origin at the cluster center. Only the top right corner is shown due to the system symmetry. The field is directed along the Z axis. The dipolar coupling constant increases from left to right: (a), (d), and (g) $\lambda = 1$; (b), (e), and (h) $\lambda = 3$; and (c), (f), and (i) $\lambda = 5$. The *average* volume fraction of particles increases from top to bottom: [(a)–(c)] $\varphi_{ex} = 0.002$, [(d)–(f)] $\varphi_{ex} = 0.05$, and [(g)–(i)] $\varphi_{ex} = 0.15$.

[κ in Eqs. (10) and (11)] decreases. This is very similar to the behavior of magnetic droplets in ferroemulsions [34] and can explain the anomalous increase of the cluster magnetization seen in Fig. 4(f). The haloing is still present at larger average concentrations. However, an important difference is that at higher average volume fractions the inhomogeneity of the local concentration decreases. In the densest environment with average particle concentration $\varphi_{ex} = 0.15$, the local particle concentration near the cluster surface is always $\varphi_{ex,\,loc} \geqslant 0.1$. Correspondingly, variations of μ_{ex} in the vicinity of the cluster get smaller. As a result, BMM (which assumes system homogeneity) works much better for concentrated LCM samples.

V. CONCLUSIONS

In this work, the equilibrium magnetic response of a binary superparamagnetic mixture was studied both theoretically and

numerically (with the help of Langevin dynamic simulations). One component of the mixture is a spherical nanocluster, consisting of immobilized magnetically isotropic single-domain particles. The cluster is submerged in a superparamagnetic medium, which itself constitutes an ensemble of single-domain particles in a nonmagnetic matrix. Two cases were considered separately. In the first case (SCM), particles of the surrounding medium were spatially immobilized, although they fully retained rotational degrees of freedom. This case allowed us to neglect possible effects of Brownian motion and particle aggregation. In the second case (LCM), particles in the medium had both translation and rotational degrees of freedom. It was shown that the magnetostatic response of the SCM system can be accurately described theoretically within the BMM approach [Eqs. (10)–(16)] if the nonlinear permeabilities of individual mixture components are known. It was also shown that MMF predictions for permeabilities [Eqs. (20)

and (21)] give an accurate description of the simulation data only at relatively small values of the dipolar coupling constant ($\lambda \leqslant 1$). The situation changes qualitatively for the LCM system. If the average particle concentration in the medium is low enough, magnetization of the mixture grows anomalously fast with the field (compared to BMM prediction). The apparent reason for this growth is the so-called haloing effect: the gradient field of the magnetized nanocluster leads to the local redistribution of particles in the surrounding medium. It was shown that particles form concentrated clouds near the cluster poles, effectively reducing the demagnetization effect and making it more susceptible to the applied field. A strong dependence of the haloing effect on the intensity of dipole-dipole interactions was revealed.

We can conclude that an accurate theoretical description of the magnetostatic response of a binary superparamagnetic mixture at $\lambda > 1$ cannot simply assume spatial homogeneity of the system's magnetic properties. The local inhomogeneity of the cluster field and the subsequent drift-diffusion particle transport must be explicitly taken into account. In practice, it will require the solution of a combined magnetodiffusive boundary-value problem similar to those previously considered in Refs. [54,55]. The solution of this problem is left for future studies.

APPENDIX A: APPROXIMATION OF MAGNETICALLY ISOTROPIC NANOPARTICLES

Let us give here a more detailed explanation of our particles being "magnetically isotropic."

The simplest and most common model for internal magnetic anisotropy of single-domain particles is the easy axis anisotropy [56]. It assumes that the particle possesses a special internal direction (easy axis) which can be characterized by a unit vector $\hat{n}$. The orientational coupling between the axis and the magnetic moment of any given particle is described by the potential

$$U_a = -Kv(\hat{m} \cdot \hat{n})^2, \tag{A1}$$

where K is the particle anisotropy constant, $\hat{m} = \vec{m}/m$. The interplay between anisotropy and thermal fluctuations is described by the dimensionless anisotropy parameter

$$\sigma = \frac{Kv}{k_BT}. \tag{A2}$$

For a 10 nm particle with $K \sim 10^4$ J/m^3, the anisotropy parameter is $\sigma \sim 1$.

It is known that the variation in σ strongly affects the *dynamic* magnetic response of single-domain particles in different matrices [57,58]. However, in this work we are interested only in the equilibrium magnetic response to a *static* applied field. And it is known that equilibrium magnetization

curves of superparamagnetic particles suspended in a liquid simply do not depend on σ [32]. The situation becomes more complicated if particles are immobilized in a solid carrier. In principle, now one has to take into account the "magnetic texture" of the system, i.e., the specific orientational distribution of the particles' easy axes. The texture can be created by applying a strong field during the synthesis stage and can have a major impact on the system magnetic response [33,59]. However, nontextured composites with a random and uniform distribution of easy axes are more similar to liquid superparamagnets; their initial magnetic response also does not depend on the anisotropy parameter σ [32,60]. Increasing σ can lower the magnetic response at larger fields (at $\xi_0 > 2$), but it will not affect the magnetization curve qualitatively [38]. Taking all this into consideration, we decided to investigate here only the limiting case $\sigma \ll 1$; that is, in zero field all internal orientations of magnetic moments are equiprobable. This approach allows us to considerably simplify both the theoretical treatment and the simulation protocol. We believe that all the results obtained here for magnetically isotropic systems can be extrapolated to liquids and nontextured solids with finite σ.

APPENDIX B: SIMULATION DETAILS

In a numerical realization of our mixture model, we consider a cubic simulation box with length $l = V_{\text{tot}}^{1/3}$. The cluster is placed in the center of this box. Its position does not change during the simulation. Three-dimensional periodic boundary conditions are imposed on a box. The field is directed along the Z axis. All the results reported are obtained using the ESPRESSO 4.1.4 simulation package [61].

Rotational motion of the ith particle is governed by the Langevin equation

$$J^*\frac{d\vec{\omega}_i^*}{dt^*} = \vec{\tau}_i^* - \gamma^{*R}\vec{\omega}_i^* + \vec{\eta}_i^{*R}, \quad \frac{d\vec{m}_i}{dt^*} = \vec{\omega}_i^* \times \vec{m}_i. \tag{B1}$$

For the LCM, translational motion of the ith particle in a viscous carrier is additionally described by an analogous equation:

$$\frac{d\vec{v}_i^*}{dt^*} = \vec{f}_i^* - \gamma^{*T}\vec{v}_i^* + \vec{\eta}_i^{*T}. \tag{B2}$$

All simulations are performed using reduced quantities, denoted here by an asterisk. They are formally introduced through the usage of three parameters: the thermal energy k_BT, the diameter of a single particle d, and the mass of a single particle $\mathfrak{M}$. Specifically, $\vec{v}_i^* = \vec{v}_i\sqrt{\mathfrak{M}/k_BT}$ and $\vec{\omega}_i^* = \vec{\omega}_i\sqrt{\mathfrak{M}d^2/k_BT}$ are the reduced linear and angular velocities, respectively. $J^* = J/\mathfrak{M}d^2$ is the reduced moment of inertia, and $\gamma^{*T} = \gamma^T\sqrt{d^2/\mathfrak{M}k_BT}$ and $\gamma^{*R} = \gamma^R\sqrt{1/d^2\mathfrak{M}k_BT}$ are the reduced translational and rotational friction coefficients. $\vec{\eta}_i^{*R}$ and $\vec{\eta}_i^{*T}$ are the random force and torque, which have zero mean values and satisfy the standard fluctuation-dissipation relationship [62]

$$\langle\eta_{i\alpha}^{*T(R)}(t_1^*)\eta_{j\beta}^{*T(R)}(t_2^*)\rangle = 2\gamma^{*T(R)}\delta_{\alpha\beta}\delta_{ij}\delta^*(t_1^* - t_2^*), \tag{B3}$$

where α and β denote Cartesian vector components, $\delta^*(t^*)$ is the Dirac delta function, δ_{ij} is the Kronecker delta, and

the reduced time is $t^* = t\sqrt{k_B T / \mathfrak{M} d^2}$. $\vec{\tau}_i^* = \mu_0 [\vec{m}_i \times (\vec{H}_0 + \vec{H}_{dd}(i))] / k_B T$ is the reduced magnetic torque acting on a given particle, and $\vec{H}_{dd}(i) = -(1/\mu_0) \sum_{j \neq i} \partial U_{dd}(i, j) / \partial \vec{m}_i$ is the sum of all dipolar fields in the particle center. $\vec{f}_i^* = -(d/k_B T) \sum_{j \neq i} \partial [U_{dd}(i, j) + U_{\text{WCA}}(i, j)] / \partial \vec{r}_i$ is the total reduced force on the particle, where $U_{\text{WCA}}(i, j)$ is the Weeks-Chandler-Andersen (WCA) pair potential that models the steric repulsion between particles [63]:

$$U_{\text{WCA}}(i, j) = \begin{cases} U_{LJ}(r_{ij}) - U_{LJ}(r_{\text{cut}}), & r_{ij} < r_{\text{cut}}, \\ 0, & r_{ij} \geqslant r_{\text{cut}}, \end{cases} \quad \text{(B4)}$$

$$U_{LJ}(r) = 4\varepsilon \left[\left(\frac{d}{r} \right)^{12} - \left(\frac{d}{r} \right)^6 \right], \quad \text{(B5)}$$

where U_{LJ} is the Lennard-Jones potential and $r_{\text{cut}} = 2^{1/6} d$.

The forces and torques due to long-range dipole-dipole interactions are computed using the dipolar P^{3}M algorithm with "metallic" boundary conditions [64]. All the results are reported for $J^* = \gamma_R^* = \gamma_T^* = \varepsilon^* = 1$, and the simulation time step is $\Delta t^* = 0.01$. Typically, the first 2×10^5 time steps are used for system equilibration, and the subsequent production run lasts for at least another 8×10^5 time steps.

[1] M. I. Shliomis, Magnetic fluids, Sov. Phys. Usp. **17**, 153 (1974).

[2] G. Bossis, S. Lacis, A. Meunier, and O. Volkova, Magnetorheological fluids, J. Magn. Magn. Mater. **252**, 224 (2002).

[3] R. Weeber, M. Hermes, A. M. Schmidt, and C. Holm, Polymer architecture of magnetic gels: A review, J. Phys.: Condens. Matter **30**, 063002 (2018).

[4] C. Bellan and G. Bossis, Field dependence of viscoelastic properties of mr elastomers, Int. J. Mod. Phys. B **16**, 2447 (2002).

[5] K. Zimmermann, V. Naletova, I. Zeidis, V. Böhm, and E. Kolev, Modelling of locomotion systems using deformable magnetizable media, J. Phys.: Condens. Matter **18**, S2973 (2006).

[6] N. Bock, A. Riminucci, C. Dionigi, A. Russo, A. Tampieri, E. Landi, V. A. Goranov, M. Marcacci, and V. Dediu, A novel route in bone tissue engineering: Magnetic biomimetic scaffolds, Acta Biomater. **6**, 786 (2010).

[7] S. Abramchuk, E. Kramarenko, D. Grishin, G. Stepanov, L. Nikitin, G. Filipcsei, A. Khokhlov, and M. Zrínyi, Novel highly elastic magnetic materials for dampers and seals: Part II. Material behavior in a magnetic field, Polym. Adv. Technol. **18**, 513 (2007).

[8] W. Cherief, Y. Avenas, S. Ferrouillat, A. Kedous-Lebouc, L. Jossic, and M. Petit, Parameters affecting forced convection enhancement in ferrofluid cooling systems, Appl. Therm. Eng. **123**, 156 (2017).

[9] W. Huang, C. Shen, S. Liao, and X. Wang, Study on the ferrofluid lubrication with an external magnetic field, Tribol. Lett. **41**, 145 (2011).

[10] R. Tietze, S. Lyer, S. Dürr, T. Struffert, T. Engelhorn, M. Schwarz, E. Eckert, T. Göen, S. Vasylyev, W. Peukert, F. Wiekhorst, L. Trahms, A. Dörfler, and C. Alexiou, Efficient drug-delivery using magnetic nanoparticles–biodistribution and therapeutic effects in tumour bearing rabbits, Nanomedicine **9**, 961 (2013).

[11] E. A. Périgo, G. Hemery, O. Sandre, D. Ortega, E. Garaio, F. Plazaola, and F. J. Teran, Fundamentals and advances in magnetic hyperthermia, Appl. Phys. Rev. **2**, 041302 (2015).

[12] Z. W. Tay, P. Chandrasekharan, A. Chiu-Lam, D. W. Hensley, R. Dhavalikar, X. Y. Zhou, E. Y. Yu, P. W. Goodwill, B. Zheng, C. Rinaldi, and S. M. Conolly, Magnetic particle imaging-guided heating in vivo using gradient fields for arbitrary localization of magnetic hyperthermia therapy, ACS Nano **12**, 3699 (2018).

[13] R. E. Rosensweig, *Ferrohydrodynamics* (Cambridge University Press, Cambridge, UK, 1985).

[14] P. Bender, D. Honecker, and L. Fernández Barquín, Supraferromagnetic correlations in clusters of mag-

netic nanoflowers, Appl. Phys. Lett. **115**, 132406 (2019).

[15] F. Ludwig, O. Kazakova, L. F. Barquín, A. Fornara, L. Trahms, U. Steinhoff, P. Svedlindh, E. Wetterskog, Q. A. Pankhurst, P. Southern *et al.*, Magnetic, structural, and particle size analysis of single-and multi-core magnetic nanoparticles, IEEE Trans. Magn. **50**, 1 (2014).

[16] V. Socoliuc, M. Avdeev, V. Kuncser, R. Turcu, E. Tombácz, and L. Vekas, Ferrofluids and bio-ferrofluids: Looking back and stepping forward, Nanoscale **14**, 4786 (2022).

[17] D. Borin, G. Stepanov, and E. Dohmen, Hybrid magnetoactive elastomer with a soft matrix and mixed powder, Arch. Appl. Mech. **89**, 105 (2019).

[18] P. A. Sánchez, O. V. Stolbov, S. S. Kantorovich, and Y. L. Raikher, Modeling the magnetostriction effect in elastomers with magnetically soft and hard particles, Soft Matter **15**, 7145 (2019).

[19] T. Becker, K. Zimmermann, D. Y. Borin, G. Stepanov, and P. Storozhenko, Dynamic response of a sensor element made of magnetic hybrid elastomer with controllable properties, J. Magn. Magn. Mater. **449**, 77 (2018).

[20] L. Fischer and A. M. Menzel, Magnetically induced elastic deformations in model systems of magnetic gels and elastomers containing particles of mixed size, Smart Mater. Struct. **30**, 014003 (2021).

[21] C. Magnet, P. Kuzhir, G. Bossis, A. Meunier, L. Suloeva, and A. Zubarev, Haloing in bimodal magnetic colloids: The role of field-induced phase separation, Phys. Rev. E **86**, 011404 (2012).

[22] J. Viota, F. González-Caballero, J. Durán, and A. Delgado, Study of the colloidal stability of concentrated bimodal magnetic fluids, J. Colloid Interface Sci. **309**, 135 (2007).

[23] M. T. López-López, A. Y. Zubarev, and G. Bossis, Repulsive force between two attractive dipoles, mediated by nanoparticles inside a ferrofluid, Soft Matter **6**, 4346 (2010).

[24] M. Khelfallah, Magnetic properties of ferrofluids of self-assembled nano-magnets, Ph.D. thesis, Sorbonne University, 2023.

[25] V. M. Buzmakov and A. F. Pshenichnikov, On the structure of microaggregates in magnetite colloids, J. Colloid Interface Sci. **182**, 63 (1996).

[26] R. Rosensweig, Magnetorheological particle clouds, J. Magn. Magn. Mater. **479**, 301 (2019).

[27] A. F. Pshenichnikov and A. S. Ivanov, Magnetophoresis of particles and aggregates in concentrated magnetic fluids, Phys. Rev. E **86**, 051401 (2012).

[28] D. Borin, A. Zubarev, D. Chirikov, R. Müller, and S. Odenbach, Ferrofluid with clustered iron nanoparticles: Slow relaxation of rheological properties under joint action of shear flow and magnetic field, J. Magn. Magn. Mater. **323**, 1273 (2011).

[29] C. P. Bean and J. D. Livingston, Superparamagnetism, J. Appl. Phys. **30**, S120 (1959).

[30] B. Huke and M. Lücke, Magnetic properties of colloidal suspensions of interacting magnetic particles, Rep. Prog. Phys. **36**, 1731 (2004).

[31] A. O. Ivanov, V. S. Zverev, and S. S. Kantorovich, Revealing the signature of dipolar interactions in dynamic spectra of polydisperse magnetic nanoparticles, Soft Matter **12**, 3507 (2016).

[32] E. A. Elfimova, A. O. Ivanov, and P. J. Camp, Static magnetization of immobilized, weakly interacting, superparamagnetic nanoparticles, Nanoscale **11**, 21834 (2019).

[33] D. I. Radushnov, A. Y. Solovyova, and E. A. Elfimova, Structure and magnetization of a magnetoactive ferrocomposite, Nanoscale **14**, 10493 (2022).

[34] A. O. Ivanov and O. B. Kuznetsova, Nonmonotonic field-dependent magnetic permeability of a paramagnetic ferrofluid emulsion, Phys. Rev. E **85**, 041405 (2012).

[35] I. M. Subbotin, Magnetic permeability of inverse ferrofluid emulsion: An influence of interdroplet interaction, Magnetohydrodynamics **54**, 131 (2018).

[36] I. M. Subbotin, Magnetic permeability of inverse ferrofluid emulsion: Nonlinear ferrofluid magnetization law, J. Magn. Magn. Mater. **502**, 166524 (2020).

[37] A. Zakinyan and I. Arefyev, Thermal conductivity of emulsion with anisotropic microstructure induced by external field, Colloid Polym. Sci. **298**, 1063 (2020).

[38] A. A. Kuznetsov, Equilibrium magnetization of a quasispherical cluster of single-domain particles, Phys. Rev. B **98**, 144418 (2018).

[39] H. Fricke, The Maxwell-Wagner dispersion in a suspension of ellipsoids, J. Phys. Chem. **57**, 934 (1953).

[40] A. F. Pshenichnikov, V. V. Mekhonoshin, and A. V. Lebedev, Magneto-granulometric analysis of concentrated ferrocolloids, J. Magn. Magn. Mater. **161**, 94 (1996).

[41] A. O. Ivanov and O. B. Kuznetsova, Magnetic properties of dense ferrofluids: An influence of interparticle correlations, Phys. Rev. E **64**, 041405 (2001).

[42] A. O. Ivanov and O. B. Kuznetsova, Magnetogranulometric analysis of ferrocolloids: Second-order modified mean field theory, Colloid J. **68**, 430 (2006).

[43] M. Krekhova, T. Lang, R. Richter, and H. Schmalz, Thermoreversible hydroferrogels with tunable mechanical properties utilizing block copolymer mesophases as template, Langmuir **26**, 19181 (2010).

[44] E. A. Elfimova, L. Y. Iskakova, A. Y. Solovyova, and A. Y. Zubarev, Theory of static magnetization of magnetopolymer composites: The second virial approximation, Phys. Rev. E **104**, 054616 (2021).

[45] Z. Wang, C. Holm, and H. W. Müller, Molecular dynamics study on the equilibrium magnetization properties and structure of ferrofluids, Phys. Rev. E **66**, 021405 (2002).

[46] G. Pessot, M. Schümann, T. Gundermann, S. Odenbach, H. Löwen, and A. M. Menzel, Tunable dynamic moduli of magnetic elastomers: From characterization by x-ray micro-computed tomography to mesoscopic modeling, J. Phys.: Condens. Matter **30**, 125101 (2018).

[47] A. O. Ivanov, Z. Wang, and C. Holm, Applying the chain formation model to magnetic properties of aggregated ferrofluids, Phys. Rev. E **69**, 031206 (2004).

[48] V. S. Mendelev and A. O. Ivanov, Ferrofluid aggregation in chains under the influence of a magnetic field, Phys. Rev. E **70**, 051502 (2004).

[49] C. Magnet, P. Kuzhir, G. Bossis, A. Meunier, S. Nave, A. Zubarev, C. Lomenech, and V. Bashtovoi, Behavior of nanoparticle clouds around a magnetized microsphere under magnetic and flow fields, Phys. Rev. E **89**, 032310 (2014).

[50] A. S. Ivanov and A. F. Pshenichnikov, Vortex flows induced by drop-like aggregate drift in magnetic fluids, Phys. Fluids **26**, 012002 (2014).

[51] A. A. Kuznetsov and I. A. Podlesnykh, Magnetophoretic equilibrium of a polydisperse ferrofluid, Nanomaterials **11**, 2849 (2021).

[52] A. F. Pshenichnikov, E. A. Elfimova, and A. O. Ivanov, Magnetophoresis, sedimentation, and diffusion of particles in concentrated magnetic fluids, J. Chem. Phys. **134**, 184508 (2011).

[53] A. A. Kuznetsov and A. F. Pshenichnikov, Sedimentation equilibrium of magnetic nanoparticles with strong dipole-dipole interactions, Phys. Rev. E **95**, 032609 (2017).

[54] O. Lavrova, V. Polevikov, and L. Tobiska, Modeling and simulation of magnetic particles diffusion in a ferrofluid layer, Magnetohydrodynamics **52**, 439 (2016).

[55] O. Lavrova and V. Polevikov, Numerical study of the shielding properties of a ferrofluid taking into account magnitophoresis and particle interaction, Math. Model. Anal. **27**, 161 (2022).

[56] W. T. Coffey and Y. P. Kalmykov, Thermal fluctuations of magnetic nanoparticles: Fifty years after Brown, J. Appl. Phys. **112**, 121301 (2012).

[57] I. S. Poperechny, Y. L. Raikher, and V. I. Stepanov, Dynamic magnetic hysteresis in single-domain particles with uniaxial anisotropy, Phys. Rev. B **82**, 174423 (2010).

[58] P. Ilg and M. Kröger, Longest relaxation time versus maximum loss peak in the field-dependent longitudinal dynamics of suspended magnetic nanoparticles, Phys. Rev. B **106**, 134433 (2022).

[59] Y. L. Raikher, The magnetization curve of a textured ferrofluid, J. Magn. Magn. Mater. **39**, 11 (1983).

[60] V. Schaller, G. Wahnström, A. Sanz-Velasco, S. Gustafsson, E. Olsson, P. Enoksson, and C. Johansson, Effective magnetic moment of magnetic multicore nanoparticles, Phys. Rev. B **80**, 092406 (2009).

[61] F. Weik, R. Weeber, K. Szuttor, K. Breitsprecher, J. de Graaf, M. Kuron, J. Landsgesell, H. Menke, D. Sean, and C. Holm, Espresso 4.0–an extensible software package for simulating soft matter systems, Eur. Phys. J.: Spec. Top. **227**, 1789 (2019).

[62] W. T. Coffey, Y. P. Kalmykov, and J. T. Waldron, *The Langevin Equation: With Applications to Stochastic Problems in Physics, Chemistry and Electrical Engineering* (World Scientific, Singapore, 2004).

[63] J. D. Weeks, D. Chandler, and H. C. Andersen, Role of repulsive forces in determining the equilibrium structure of simple liquids, J. Chem. Phys. **54**, 5237 (1971).

[64] J. J. Cerda, V. Ballenegger, O. Lenz, and C. Holm, P³M algorithm for dipolar interactions, J. Chem. Phys. **129**, 234104 (2008).